Int J Adv Manuf Technol (2017) 89:27–43
DOI 10.1007/s00170-016-9046-x

ORIGINAL ARTICLE

Prediction and optimization of weld bead geometry for electron beam welding of AISI 304 stainless steel

Arpith Siddaiah[1] · **B. K. Singh**[1] · **P. Mastanaiah**[2]

Received: 1 July 2015 / Accepted: 13 June 2016 / Published online: 23 June 2016

Abstract Electron beam welding, though considered a sophisticated welding process, still requires the operator to first carry out several trial welds to find the right combination of welding parameters based on intuition and experience. This archaic method is often unreliable, leading to unproductive manufacturing lead time, man hours, quality control tests, and material wastage. The current study eliminates this "trial and error" method by providing a reliable model which can predict the right combination of weld parameters to achieve a high-quality weld. Beads on plate welds were carried out on AISI 304 stainless steel plates using a low-kilovolt electron beam welding (EBW) machine. A model that can predict weld bead geometry and provide optimized output for minimum weld area condition without compromising on weld quality was developed. Experimental data were collected as per full factorial design of experiments, and the levels for each input parameter were established through pilot experiments. A multivariate regression analysis has been conducted to establish a relationship between four weld input parameters (three levels each) and four weld bead responses. Response surface methodology (RSM) has been used to study the interrelationship between input parameters and their effect on each response variable. Further, minimization of weld cross-sectional area was done using genetic algorithm for maximum penetration and minimum weld area condition. The optimized mathematical model convincingly establishes that the focusing current is a significant input parameter with very high influence over the weld bead geometry. Extensive material characterization and mechanical tests have been carried out to validate the regressed input-output relationship and the optimized mathematical model.

Keywords Electron beam welding · Weld bead geometry · Stainless steel · Full factorial design of experiment · Multiple regression analysis · Response surface methodology

Abbreviations

ANOVA	Analysis of variance
BBW	Back bead width
BH	Bead height
BP	Bead penetration
BW	Bead width
D	Standoff distance/work to chamber top distance (mm)
EBW	Electron beam welding
F	Focusing current (A)
HAZ	Heat-affected zone
I	Beam current (mA)
RSM	Response surface methodology
R-sq, R^2	Coefficient of correlation
S	Welding speed/beam spot travel (m/min)
SE	Standard error
T	Thickness of plate (mm)
V	Accelerating voltage (kV)

✉ Arpith Siddaiah
arpith4@gmail.com

[1] Department of Production Engineering, Birla Institute of Technology, Mesra, Ranchi 835215, India

[2] Special Fabrication Division, Directorate of Engineering, Defence Research and Development Laboratory, DRDO, Hyderabad 500058, India

1 Introduction

Welding operations require an operator to have considerable skill and experience necessary to select the optimal combination of welding parameters for specific application. The input parameter selection process is further complicated by the fact that optimal settings are affected by base material, electrode composition, welding position, and quality requirements. Electron beam welding (EBW) is a technique that has eliminated many such shortcomings [18]. The precision, accuracy, and repeatability of welds that are achieved by EBW cannot be consistently replicated by any expert welder [11].

EBW is a fusion welding process which produces weld by imposing a beam of high-energy electrons to heat the joint. The kinetic energy of these electrons is transferred to the work material, which produces intense heating resulting in melting and fusion [19]. Li and Gobbi [15, 16] discuss that welding in high vacuum condition helps to avoid material contamination and yields deep penetration. This also ensures a minimum size of the fusion zone (FZ) and the heat-affected zone (HAZ) with minimal distortion and residual stresses. EBW yields welds that are deep, narrow, and defect free with very high joining rates. The possible mechanism behind creation of these deep welds is described by Schultz [20].

A fusion zone is generally characterized by geometrical features, namely, bead width (BW), bead height (BH), bead penetration (BP), and back bead width (BBW) as identified by Benyounis [1]. The first attempt to model the distinct "nail head" appearance of the weld bead cross section was made by Klykov [13]. He combined a depth source which describes the keyhole effects and its energy-related transfer with a surface source, representing the plume radiation on the workpiece surface.

Developing a methodology to mathematically model a relation between the input-output variables for a welding process is a very important aspect before analysis or optimization. All experimental analyses require a standard experimental procedure to be designed to help establish the required relationship. Dashatan [2] investigates the effect of friction stir spot welding parameters on mechanical properties of welded specimens using full factorial design of experiment to be sure that the relationship is not influenced by interactions present among the input parameters. It is seen that full factorial design is best way to proceed when a new process or material is to be analyzed and/or if a high degree of interrelationship is present between the input parameters. Jean [8] presents the application of Taguchi's orthogonal experimental method to effectively and efficiently design an electron beam welding treatment process of high multiple performance characteristics.

A full factorial design would require all possible combination of experiments to be conducted, while the widely used Taguchi's design of experiments gives a selective combination of input parameters with minimum number of experimental trials. Full factorial design is seen to be advantageous when all effects and interactions between the input parameter are to be analyzed. One limitation of this design is the large size of the design space, and hence, constraints on parameter combinations are difficult to include [10].

Genetic algorithm (GA) is an optimization technique based on the biological evolution process. Holland [7] used a similar analogy to develop solutions to complex optimization problems. He indicates that the notable feature of genetic algorithm is that it emulates the biological system's characteristics like self-repair and reproduction. Khan [12] show that GAs differ from simulated annealing in the fact that the optimal solution is selected from a population of solutions and not from one solution which is computed based on a probability. Jha [9] used electron beam butt-welded specimens of American Iron and Steel Institute (AISI) 304 plates to compare and study genetic algorithm neural network (GANN) and back propagation neural network (BPNN) optimization techniques for optimization of weld profile. He defined weld bead profile in terms of bead width, depth of weld penetration, yield strength, and ultimate tensile strength. He found that GANN outperformed BPNN in both forward and reverse mapping of weld profile. Hence, genetic algorithm is observed to be the best technique for weld bead optimization and also to study the effect of new parameters and their interactions.

Madhusudan [17] investigates the microstructure and mechanical properties of some of the most widely used grades of steel like AISI 304, 430, and 2205. These materials have been studied for similar and dissimilar welded joints on an electron beam welding machine, and the weld behaviors have been weld reported. Even high-strength materials such as titanium- [21] and nickel-based super

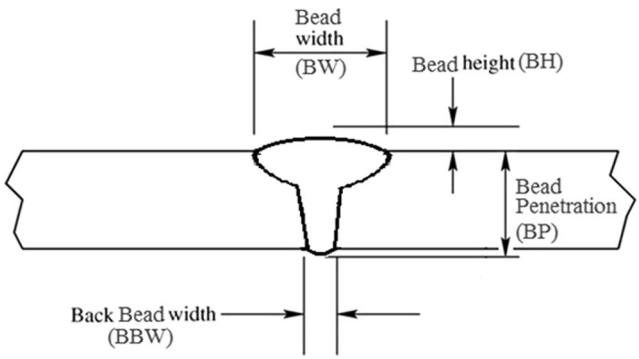

Fig. 1 Schematic representation of weld bead geometry

Table 1 Input parameter levels

Material (thickness)	Acceleration voltage (*V*), kV	Beam current (*I*), mA	Welding speed (*S*), m/min	Focusing current (*J*), A
SS304 (2 mm)	Level (−1) = 40	Level (−1) = 14	Level (−1) = 0.8	Level (−1) = 96 SF Three sub-levels 95–97
	Level (0) = 45	Level (0) = 16	Level (0) = 1.0	Level (0) = 101 SF Three sub-levels 100–102
	Level (+1) = 50	Level (+1) = 18	Level (+1) = 1.2	Level (+1) = 107 SF Three sub-levels 106–108

alloys [6] have been analyzed for their microstructure and mechanical properties. Although there is an abundance of research database on the mechanical behavior of various stainless steel grades, steel single-crystal [3] and other high-strength alloys for electron beam welding, there is still a paucity of data and methodology of predicting the weld bead geometry accurately for the same.

Dey [4, 5] conducted a study for bead-on-plate electron beam welding of 5-mm-thick austenitic stainless steel plates of ASS-304 grade and aluminum plates of Al-1100 grade. The primary aim of his study was to minimize weldment area by applying genetic algorithm optimization without sacrificing the quality of the weld. This was accomplished by minimizing the weld bead width and height and maximizing the weld penetration. One major shortcoming in both the above-cited researches is that the focusing current has not been considered as an input parameter. Koleva [14] have considered the focus current in their quality analysis of weld beads in EBW, but they have kept it at a constant value without considering the effect on weld bead geometry due to its variation.

Knowledge and control of input variables that define an EB-welded bead profile is essential to consistently produce welds of satisfactory quality. Since these input parameters are not completely independent of one another, changing one variable requires changing one or more of the others to produce the desired results. Bead cross-sectional area along with the bead height and bead width determines the amount of residual stresses and distortion of the welded structure. Cooling rate of the weldment and weld cracking are also seen to be related to the profile of the bead. Hence, the mechanical properties of welded structure are highly dependent on the size and shape of the weldment.

A deep high-quality weld requires the appropriate values of beam power, beam profile, welding velocity, and focal point location relative to the workpiece [18]. The study undertaken provides a model that predicts the bead geometry as a function of weld input parameters and discusses the effect of focusing current. It also gives an insight into optimization of different welding parameters to achieve the condition of minimum cross-sectional area weld bead with maximum penetration. Further, the study proves through extensive material characterization and mechanical tests that this minimized weld bead is mechanically sound and that the weld quality has not been compromised.

2 Experimentation and data collection

Electron beam welding machine used in the present work is a low-kilovolt EBW (65 kV, 300 mA) having 1-m^3 vacuum chamber. The input process parameters that affect the bead geometry of an electron beam-welded specimen were identified through pilot experiments as −acceleration voltage (*V*), beam current (*I*), welding speed (*S*), standoff distance (*D*), focusing current (*F*), and thickness of work (*T*).

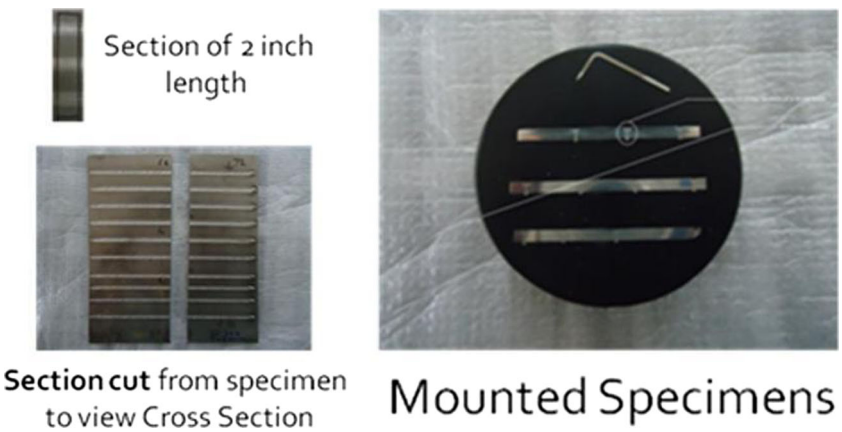

Fig. 2 Cutout section from bead on plate-welded specimen and its final mounted specimen

Table 2 Full factorial experimental data of SS304

SS304 material Run order	Acceleration voltage (*V*), kV	Beam current (*I*), mA	Welding speed (*S*), m/min	Focusing current (*F*), A	Bead height (BH), mm	Bead width (BW), mm	Weld penetration (WP), mm	Back bead width (BBW), mm
1	40	14	0.8	95	0.17	1.37	1.84	0.57
2	40	14	0.8	96	0.18	1.31	1.93	0.45
3	40	14	0.8	97	0.14	1.38	1.04	0.72
4	40	14	1.0	95	0.16	1.32	1.65	0.53
5	40	14	1.0	96	0.10	1.27	1.66	0.42
6	40	14	1.0	97	0.07	1.37	1.22	0.39
7	40	14	1.2	95	0.10	1.28	1.46	0.55
8	40	14	1.2	96	0.13	1.18	1.53	0.43
9	40	14	1.2	97	0.11	1.17	0.89	0.34
10	40	16	0.8	97	0.14	1.48	1.59	0.41
11	40	16	0.8	96	−0.16	1.10	2.48	0.49
12	40	16	0.8	95	−0.15	1.17	2.61	0.46
13	40	16	1.0	95	0.17	1.39	1.96	0.40
14	40	16	1.0	96	0.15	1.31	2.11	0.18
15	40	16	1.0	97	0.13	1.33	1.58	0.43
16	40	16	1.2	95	0.18	1.26	1.84	0.58
17	40	16	1.2	96	~0	0.68	1.63	0.30
18	40	16	1.2	97	~0	0.81	1.19	0.34
19	40	18	0.8	95	0.05	0.86	2.77	0.65
20	40	18	0.8	96	−0.10	1.44	2.31	0.70
21	40	18	0.8	97	0.19	1.68	2.05	0.14
22	40	18	1.0	95	−0.07	1.28	2.29	0.53
23	40	18	1.0	96	0.13	1.24	2.52	0.44
24	40	18	1.0	97	0.14	1.53	1.87	0.42
25	40	18	1.2	95	0.15	1.30	2.04	0.12
26	40	18	1.2	96	−0.12	1.10	2.53	0.56
27	40	18	1.2	97	0.13	1.35	1.59	0.42
28	45	14	0.8	100	0.14	1.69	1.59	0.83
29	45	14	0.8	101	−0.20	1.37	2.94	0.74
30	45	14	0.8	102	−0.18	1.32	2.63	0.50
31	45	14	1.0	100	0.11	1.45	1.41	0.86
32	45	14	1.0	101	0.17	1.46	1.83	0.60
33	45	14	1.0	102	0.14	1.36	2.07	0.17
34	45	14	1.2	100	0.13	1.46	1.29	0.78
35	45	14	1.2	101	0.16	1.24	1.72	0.53
36	45	14	1.2	102	0.11	1.25	1.94	0.43
37	45	16	0.8	100	0.13	1.73	1.76	0.77
38	45	16	0.8	101	−0.14	1.41	2.54	0.64
39	45	16	0.8	102	−0.09	1.42	2.48	0.57
40	45	16	1.0	100	0.08	1.75	1.57	0.84
41	45	16	1.0	101	−0.16	1.33	2.46	0.47
42	45	16	1.0	102	−0.21	1.29	2.43	0.44
43	45	16	1.2	100	0.12	1.61	1.48	0.77
44	45	16	1.2	101	0.16	1.46	2.06	0.16
45	45	16	1.2	102	−0.22	1.17	2.39	0.37
46	45	18	0.8	100	−0.10	2.06	2.53	0.54

Table 2 (continued)

SS304 material Run order	Acceleration voltage (*V*), kV	Beam current (*I*), mA	Welding speed (*S*), m/min	Focusing current (*F*), A	Bead height (BH), mm	Bead width (BW), mm	Weld penetration (WP), mm	Back bead width (BBW), mm
47	45	18	0.8	101	−0.15	1.57	2.44	0.80
48	45	18	0.8	102	−0.12	1.56	2.46	0.71
49	45	18	1.0	100	0.12	1.89	1.77	0.94
50	45	18	1.0	101	−0.08	1.40	2.56	0.62
51	45	18	1.0	102	−0.12	1.37	2.40	0.62
52	45	18	1.2	100	0.17	1.50	1.80	0.75
53	45	18	1.2	101	−0.07	1.19	2.56	0.48
54	45	18	1.2	102	−0.09	1.26	2.45	0.43
55	50	14	0.8	106	−0.08	1.67	2.45	0.42
56	50	14	0.8	107	−0.17	1.42	2.58	0.62
57	50	14	0.8	108	−0.08	1.56	2.54	0.53
58	50	14	1.0	106	0.14	1.71	1.75	0.80
59	50	14	1.0	107	−0.14	1.41	2.83	0.55
60	50	14	1.0	108	−0.22	1.38	2.46	0.47
61	50	14	1.2	106	0.15	1.51	1.64	0.80
62	50	14	1.2	107	−0.12	1.50	2.53	0.67
63	50	14	1.2	108	−0.06	1.73	2.65	0.72
64	50	16	0.8	106	0.17	1.33	2.05	0.10
65	50	16	0.8	107	0.16	1.35	2.10	0.13
66	50	16	0.8	108	−0.08	1.62	2.47	0.68
67	50	16	1.0	106	−0.04	1.60	2.49	0.47
68	50	16	1.0	107	−0.08	1.36	2.49	0.61
69	50	16	1.0	108	−0.11	1.29	2.46	0.57
70	50	16	1.2	106	0.18	1.50	2.03	0.22
71	50	16	1.2	107	−0.11	1.20	2.50	0.62
72	50	16	1.2	108	−0.10	1.23	2.45	0.60
73	50	18	0.8	106	−0.09	1.63	2.45	0.89
74	50	18	0.8	107	−0.12	1.38	2.31	0.93
75	50	18	0.8	108	−0.11	1.55	2.36	0.83
76	50	18	1.0	106	−0.04	1.73	2.51	0.78
77	50	18	1.0	107	−0.08	1.37	2.42	0.54
78	50	18	1.0	108	−0.11	1.40	2.41	0.67
79	50	18	1.2	106	−0.09	1.37	2.65	0.55
80	50	18	1.2	107	−0.08	1.17	2.34	0.53
81	50	18	1.2	108	−0.09	1.34	2.51	0.51

Similarly, the response variables that define the weld bead geometry are as identified in Fig. 1, −BH, BW, BBW, and BP. The standoff distance for the machine in use is kept constant at 283 mm, and SS304 specimens of 2-mm thickness are used. The remaining four parameters are defined as the input process parameters for the experiment.

Abrasive water jet cutting machine was used to cut SS304 specimens, which were then milled accurately to dimensions of 110 × 100 × 2 mm. The steps that lead to full factorial experiential data collection are discussed below:

2.1 Identification of process parameter levels

Pilot experiments were carried out to find the range of values for the input process parameters, which are specific to the material type and thickness. This range is the maximum (level 1), average (level 0), and minimum (level −1), for which a weld can be obtained are as shown in Table 1. It is also on the basis of these pilot experiments that the extent to which EB weld input variables affected the bead geometry was analyzed initially.

Table 3 R-sq. percent values of SS304 weld bead responses with respect to each input variable for curve estimation

Material SS304	*V*				*I*				*S*				*F*			
	BH	BW	BP	BBW	BH	BW	BP	BBW	BH	BW	BP	BBW	BH	BW	BP	BBW
Linear	16.4	13.9	21.9	8.7	4.7	0.1	12.7	0.3	3	10.5	6.2	2.9	20.2	9.8	22.5	5.6
Logarithmic	16.6	14.4	21.9	9.1	4.7	0	12.7	0.2	3	10.6	6.2	2.9	20.2	10.1	22.7	5.7
Inverse	16.7	15	21.9	9.5	4.7	0	12.6	0.1	3.1	10.1	6.2	2.8	20.1	10.4	22.3	5.8
Quadratic*	17	19.5	21.9	13.6	4.8	3.1	12.7	8.1	3.1	11.9	6.2	2.9	20.2	17.5	23.6	7.4
Cubic*	17	19.5	21.9	13.6	4.8	3.1	12.7	8.1	3.1	11.9	6.2	2.9	20.2	17.5	23.6	7.4
Compound	–	14.7	21.7	4.7	–	0	14.1	0	–	10	6	1	–	10.9	21.8	3.2
Power	–	15.2	21.8	4.9	–	0	14.1	0	–	9.5	6	1	–	11.2	21.7	3.2
S	–	15.8	21.7	5.2	–	0	14.1	0	–	8.9	5.9	0.9	–	11.5	21.5	3.3
Growth	–	14.7	21.7	4.7	–	0	14.1	0	–	10	6	1	–	10.9	21.8	3.2
Exponential	–	14.7	21.7	4.7	–	0	14.1	0	–	10	6	1	–	10.9	21.8	3.2
Logistic	–	14.7	21.7	4.7	–	0	14.1	0	–	10	6	1	–	10.9	21.8	3.2

*Best R-sq percentage for weld bead responses in consideration

2.2 Effect of focusing current

The literature review indicates that previous research papers and journals in this field [4, 5, 9] have not included the effect of focusing current (*F*) an input variable. The inclusion of focusing current as an influential parameter further complicated the selection of levels for full factorial design of experiment. This complication was due to the discreet effect the accelerating voltage had on the focusing current.

This challenge was addressed by developing a mixed sub-level design, wherein one level of voltage value was related to three levels of focusing current. The three

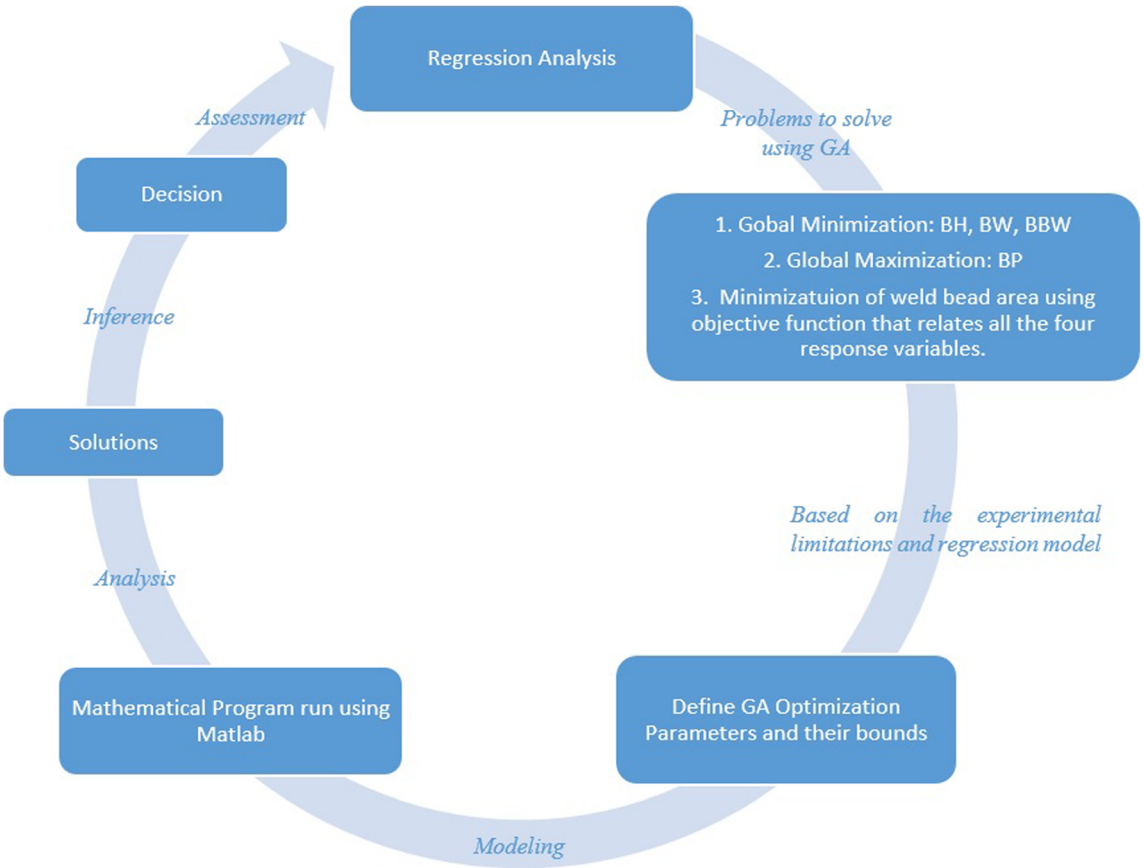

Fig. 3 Steps in mathematical formulation of the optimized problems

Table 4 GA optimization input parameters

Parameters	Values/method
Upper bounds of predictor variables	[50, 18, 1.2, 108]
Lower bounds of predictor variables	[40, 14, 0.8, 95]
Population size	$N = 100$
Number of generations	$G = 100$
Crossover probability	0.8
Mutation probability	0.2
Stall generation	50
Elite count	2
Creation function	Feasible population criterion
Scaling function	Rank-based scaling
Selection function	Roulette selection method
Mutation function	Adaptive feasible mutation
Crossover function	Scattered crossover

levels of focusing current were selected at the conditions of one above focus, surface focus, and one below focus; the values of which were decided through pilot experiments.

2.3 Design of experiment

A full factorial design of experiment with four input parameters, each of three levels with one parameter of mixed sublevel, is designed to have a treatment combination of $3^4 = 81$ combinations. The beads on plate welding for these combinations were carried in high vacuum-controlled conditions.

The bead on plate-welded specimens was further processed to mount their cross section onto 2-in-diameter cylindrical molds of 25-mm height as shown in Fig. 2. The mounted specimens were first polished using abrasive papers in the order of 240, 400, 800, 1200, and 2000 grit size followed by a 3-μm diamond paste lapping operation.

After polishing, the mounted specimens were etched using Ralph's reagent, which revealed the weld bead cross sections. The bead geometry (response) was measured in terms of BH, BW, BP, and BBW using a flash microscope as reported below in Table 2.

3 Mathematical modeling

This study is aimed at developing a model to predict the bead geometry as a function of weld input parameters. The first step toward this is curve estimation, which will indicate the type of model on which the required relationship could be built.

Table 3 shows the curve estimation done using IBM SPSS 22 software, which gives the values of coefficient of correlation (R^2) in percentage for various regression curve fit models. This table is an indication toward how each model would behave when used to fit the regression model. The R^2 values quantify how much variance in response can be explained by each predictor variable when used in the regression model. It can be observed that the quadratic and cubic models yield the best percentages of R^2, and hence, it can be inferred that one of these models is best to fit the required regression equation.

When interactions between four predictors are also considered along with the quadratic regression model, the number of terms in the equation goes up to 14. The same when used for a cubic regression model, the number of terms in the regression equation will be 22. An equation with 22 terms is clearly not a feasible one to be used under real-time condition; hence, quadratic regression curve fit model is adopted. Multiple linear regression analysis was carried out using statistical software Minitab 15 to express BH, BW, BP, and BBW in terms of V, I, S, and F. The input data used was first standardized so as to achieve normalized regression model that would be a good estimator of response variable for all ranges of input parameters.

$$\text{Bead geometry} = [\text{BH, BW, BP, BBW}] = f[V, I, S, F]$$

The general form of regressed equation including the interaction terms is as follows:

$$Y = b_0 + b_1V + b_2I + b_3S + b_4F + b_{11}V^2 + b_{22}I^2 + b_{33}S^2 + b_{44}F^2 + b_{12}VI + b_{13}VS + b_{14}VF + b_{15}IS + b_{23}IF + b_{24}SF \quad (1)$$

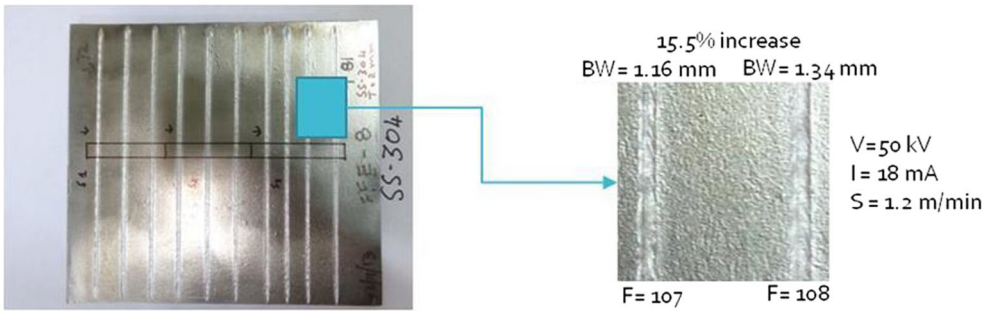

Fig. 4 Effect of focusing current as seen during pilot experiment

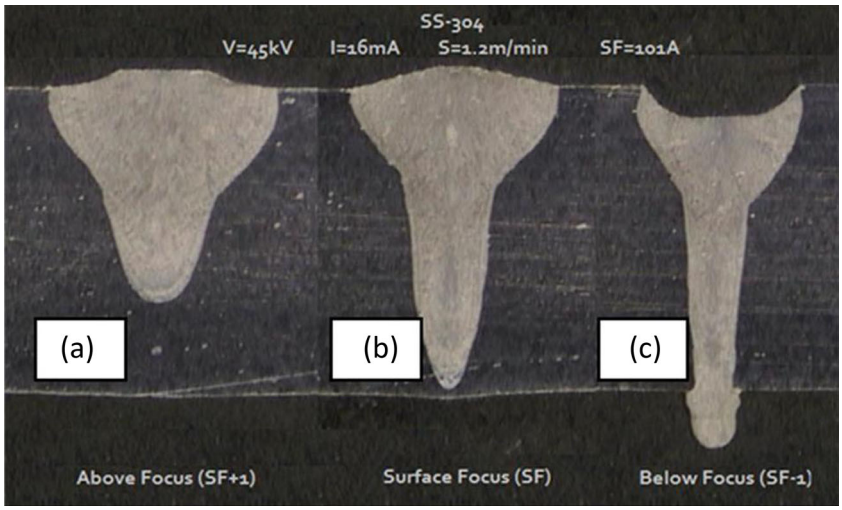

Fig. 5 The figure shows three weld beads of SS304 with input parameter change of one focus current, **a** bead obtained at one above focus, **b** bead obtained at surface focus, and **c** bead obtained at one below focus

where Y is the response variable with b_0 as the constant and b_1, b_2, b_3… are the corresponding coefficients of input parameters. The constant or intercept b_0; the linear coefficients b_1, b_2, b_3, and b_4; the squared coefficients b_{11}, b_{22}, b_{33}, and b_{44}; and the interaction term coefficients b_{12}, b_{13}, b_{14}, b_{23}, b_{24}, and b_{34} can be calculated using the following expressions [10]:

$$b_0 = \overline{Y} - b_1\overline{X_1} - b_2\overline{X_2} \tag{2}$$

$$b_1 = \frac{\sum X_i Y_i - \overline{Y}\sum X_i}{\sum X_i^2 - \overline{X}\sum X_i} \tag{3}$$

where Y_i and X_i are the i^{th} response data and predictor data, respectively, for that particular predictor variable with their data means as $\overline{Y}$ and $\overline{X}$. Similarly, values of b_{11}, b_{22}, b_{33}, b_{12}, b_{13}, b_{14}, b_{23}, b_{24}, and b_{34} can be calculated substituting their respective linear, square, or interaction terms in place of X_i.

In order to understand how the response behaves in a given direction by adjusting the design variables, response surface plots and contour plots are plotted in the next stage. These plots of the above model are critical to visualize graphically the interaction within the predictors and their effect on the responses.

4 Optimization using genetic algorithm

Genetic algorithm has been utilized for global minimization of response variables BH, BW, and BBW and global maximization of response variable BP. These extrema were then used to find an optimum weld bead with least weld cross-sectional area, which would also imply least heat-affected zone for a full penetration condition (Fig. 3).

The first step of the optimization involved finding the minimum and maximum values of individual response variables by using the established levels of input parameter as upper and lower bounds. These extrema hold true only when the responses are analyzed singularly. The fitness functions used for each response are the regressed equations of BH, BW, BP, and BBW. The optimization is done using GA optimization tool in MATLAB 7.0 2010a, and the GA parameter combinations used are listed below in Table 4.

The next challenge in optimization of weld bead was minimization of a fitness function that was derived geometrically to represent an ideal weld bead cross-sectional area; the equation representing the weld bead cross-sectional area is given by Eq. (4). This fitness function was geometrically derived to define an ideal nail-head cross section for an EB butt-welded bead.

$$\begin{aligned}\text{Area}_{\text{SS304}}(\text{BH},\ \text{BW},\ \text{BP},\ \text{BBW}) \\ = \left(\frac{\text{BW}^2 + 4\text{BH}^2}{8\text{BH}}\right)^2 \cos^{-1}\left(\frac{\text{BW}^2 - 4\text{BH}^2}{\text{BW}^2 + 4\text{BH}^2}\right) - \frac{\text{BW}^3}{16\text{BH}} + \frac{(\text{BH})(\text{BW})}{4} + \text{BW} + \frac{(\text{BP})(\text{BBW})}{2}\end{aligned} \tag{4}$$

Here, the individual extrema of each response variable that were found in the earlier optimization were used as upper and lower bounds. The bounds for cross-sectional weld area as a function of [BH, BW, BP, BBW] for SS304 are as follows:

Table 5 Statistical results of the developed regression models

Responses	Material SS304		
	R-sq. percent	Adjusted R-sq. percent	SE
BH	90.5	87.7	0.045
BW	92.3	90.1	0.049
BP	89.4	86.8	0.163
BBW	94.6	90.8	0.039

Lower bounds [−0.04, 1.05, 2.14, 0.15]
Upper bounds [0.15, 2.06, 2.83, 0.92].

5 Results and discussion

The multivariate regression analysis conducted as per 3^4 full factorial design is able to establish a relationship between four EB weld input parameters and the response variables with a reliability >90 % for each of the parameters under study. The response surface and contour plots have been used to study the interrelationship between input parameters and their effect on each response variable. Further, minimization of the weld area cross section was done using genetic algorithm optimization tool with the condition of maximum penetration and minimum weld area. The experiments and analysis conducted convincingly establish that the focusing current is a significant input parameter with very high influence over the weld bead geometry. The developed model tested for its repeatability and reliability has also been validated through extensive experiments. The results obtained for each of these stages have been discussed in detail below.

5.1 Effect of focusing current

The correlation analysis conducted on input variables indicates that the accelerating voltage is directly proportional to the focusing current. For a significance value of 95 % (p value <0.05), the Pearson's coefficient is found to be 0.983, which indicates a linear correlation. The existence of high correlation between these two input variables shows that focusing current is one of the most influential factors affecting the size and shape of the bead geometry.

The above statement was experimentally validated as seen in Fig. 4, where for an increase of one focusing current value, keeping all other input parameters constant, there was a change of 15.5 % in bead width. Further convincing evidence of this was seen from the pilot experiments, where

- For a change of one unit in focus current keeping all other input parameters at the same value, it was observed that on an average, BW changes by
  - 16.95 % (min-max 1.23 to 26 %) going above focus (surface focus +1);
  - 8.55 % (min-max 0.73 to 20 %) going below focus (surface focus −1);
  - 12 % overall for either going above or below focus.
- As shown in Fig. 5, for a change of one unit in focus current keeping all other input parameters at the same value, the BP response variable changes by
  - 7.22 % (3.5 to 56 %) going above focus;
  - 2.73 % (0.5 to 26 %) going below focus;
  - 14.69 % overall for either going above or below focus.

5.2 Mathematical modeling [10]

The statistical results of the model developed are as seen in Table 5, and the corresponding ANOVA results obtained for the model are shown below in Table 6.

A high R^2 value ranging from 89.4 to 94.6 % was observed with a low standard error value of 0.038 to

Table 6 ANOVA results of the developed regression models

Material	Response	Source	Sum of squares (Coded form)	DF	Mean square (coded form)	F ratio (calculated)	F ratio (tabulated)	p value
SS304	BH	Regression	0.8972	14	0.06409	32.04	1.908	0.00
		Residual	0.0940	47	0.002	–	–	–
	BW	Regression	1.36625	14	0.09758	45.22	1.908	0.00
		Residual	0.10144	47	0.002158	–	–	–
	BP	Regression	13.1945	14	0.94247	35.4	1.863	0.00
		Residual	1.5707	59	0.02662	–	–	–
	BBW	Regression	0.51873	14	0.03705	24.92	2.224	0.00
		Residual	0.029733	20	0.00148	–	–	–

0.16. Also, an F ratio (calculated) ranging from 24.92 to 32.04 was found to be very high when compared to the tabulated F distribution table which ranges from 1.8 to 2.22. These results indicate that the regression model developed was theoretically adequate to predict the responses BH, BW, BP, and BBW. The uncoded form of regression equations defining all four bead geometry responses in terms of V, I, S, and F are as follows:

$$\text{BH (R-sq : 90.50 \%)} = 12.8 + 1.51\,V + 0.573\,I - 2.51\,S - 1.00\,F + 0.0284\,V^2 - 0.0086\,I^2 - 0.412\,S^2 + 0.0146\,F^2 + 0.008\,VI - 0.0377\,VS - 0.0412\,VF + 0.059\,IS - 0.00709\,IF + 0.0375\,SF \quad (5)$$

$$\text{BW (R-sq : 93.10 \%)} = 378 + 16.8\,V - 1.76\,I + 8.43\,S - 14.7\,F + 0.181\,V^2 + 0.0340\,I^2 - 1.07\,S^2 + 0.142\,F^2 - 0.0381\,VI + 0.101\,VS - 0.321\,VF - 0.191\,IS + 0.0263\,IF - 0.0835\,SF \quad (6)$$

$$\text{BP (R-sq : 89.36 \%)} = -772 - 36.4\,V + 2.76\,I - 26.6\,S + 31.2\,F - 0.445\,V^2 - 0.0020\,I^2 + 1.28\,S^2 - 0.320\,F^2 + 0.0169\,VI - 0.267\,VS + 0.754\,VF + 0.0984\,IS - 0.0341\,IF + 0.332\,SF \quad (7)$$

$$\text{BBW (R-sq : 94.58 \%)} = -189 - 8.32\,V + 1.24\,I - 1.30\,S + 7.23\,F - 0.0924\,V^2 + 0.00865\,I^2 + 1.05\,S^2 - 0.0695\,F^2 + 0.0302\,VI - 0.102\,VS + 0.160\,VF - 0.279\,IS - 0.0253\,IF + 0.0789\,SF \quad (8)$$

The initial adequacy check of the model was done through linear fit test performed on the above regression equations using Minitab 15. The response plots shown in Fig. 6 indicate a linear variation of predicted responses with respect to actual

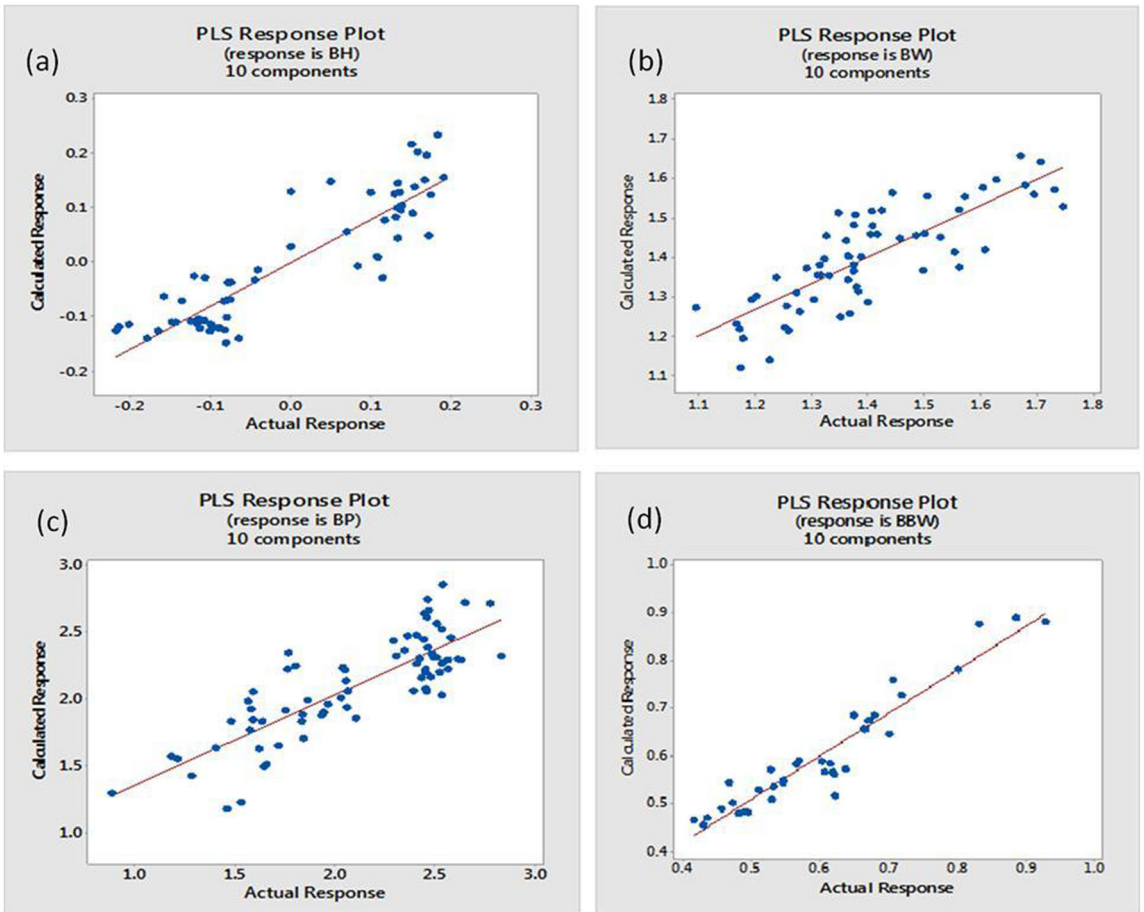

Fig. 6 Response plots

Table 7 Test case levels of input parameters

Material (thickness)	Acceleration voltage (*V*), kV	Beam current (*I*), mA	Welding speed (*S*), m/min	Focusing current (*J*), A
SS304 (2 mm)	Level (0) = 43	Level (0) = 15	Level (0) = 0.8	Level (0) = 99 SF Two sub-levels 99 and 100
	Level (1) = 48	Level (1) = 19	Level (1) = 1.0	Level (1) = 104 SF Two sub-levels 104 and 105

responses. This linear variation can be fitted around a line inclined approximately at 45^0, which indicates that the regressed model is a good predictor for the responses.

5.3 Regression model validation and adequacy check

Sixteen random experimental combinations were selected at levels as shown in Table 7. The inclusion of randomness makes sure that the model was

- Normalized, so that the model can be applied for all ranges of input values of the parameters.
- Provides a correlation between predicted and actual values of the responses with minimal residues.

The deviation analysis of predicted responses from the actual is quantified in terms of millimeter and percentage to better perceive the residues. The deviation plots as seen in Fig. 7 showed that there was a mean deviation of 10.9 % (0.012 mm) in BH, 2.9 % (0.032 mm) in BW, 9.6 % (0.22 mm) in BP, and −2.5 % (−0.0064 mm) in BBW.

This deviation analysis was an indicative of the model being adequate enough to accurately predict the bead geometry with very marginal acceptable errors, hence validates the regression equations.

5.4 Response surface and contour plots

The response surface methodology has been utilized to analyze the interacting effect of input parameters on the bead geometry. The surface and contour plots representing all six interacting terms with respect to each response variables of SS304 bead geometry is analyzed. Some major observations made from these are that

- The plots conclusively prove that focusing current varies linearly with respect to accelerating voltage for all response variables.

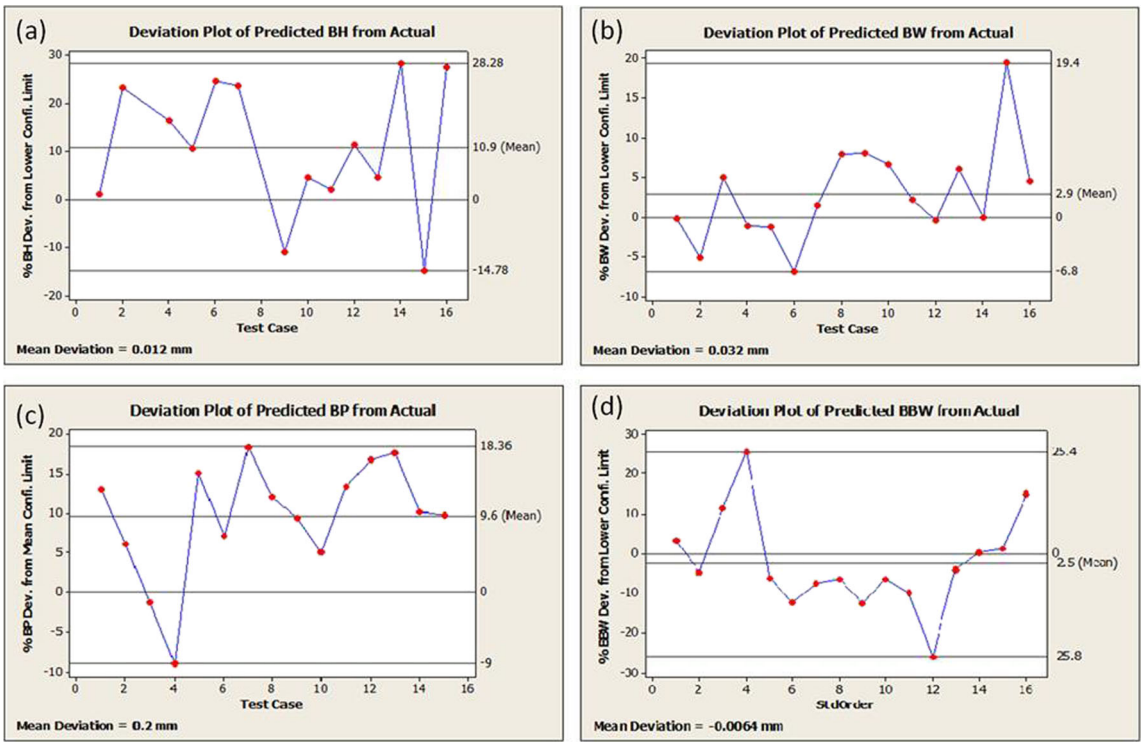

Fig. 7 Deviation plots

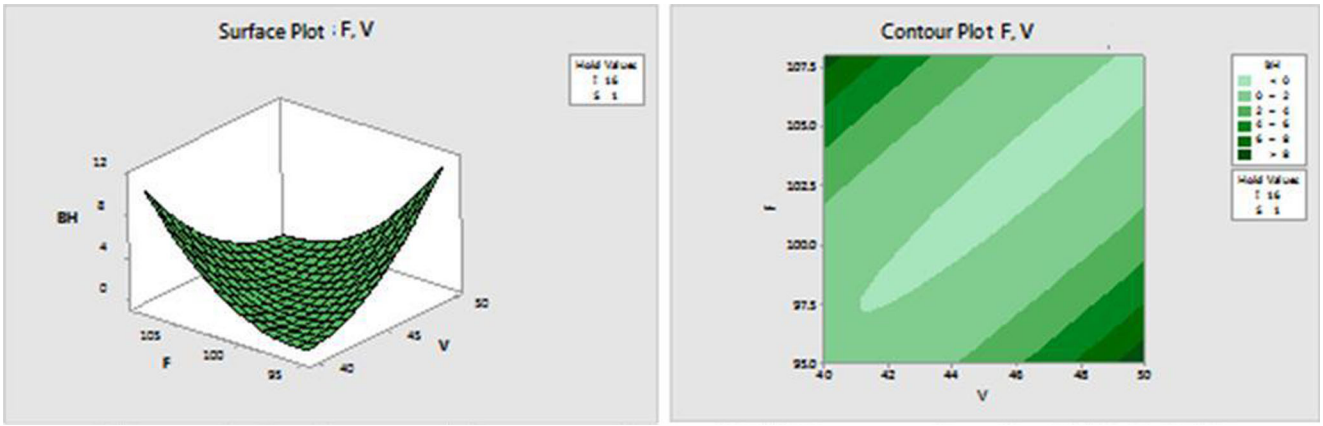

Fig. 8 Surface and contour plots of *F*-*V* interaction for BH

- The plots with respect to bead height are similar to that of bead width, and the plots with respect to bead penetration were similar to back bead width.
- Welding speed and beam current are the best parameters to be varied for making minor adjustments to the bead geometry.

The behavioral deductions drawn from few of the significant interacting input parameters are discussed in the following:

1. Focusing current (*F*) and accelerating voltage (*V*) interaction

   Figure 8 shows the surface and contour plots for interaction between focusing current and accelerating voltage with respect to response BH. Similar effects are seen in case of response BW. The plots clearly indicate a linear relation between the two predictors with focusing current increasing as accelerating voltage increases. This behavior of the input parameters is as expected since it was indicated by the correlation analysis in the initial stages of model development. The responses BH and BW are seen to be at maximum when for a particular voltage, the focusing current is at a maximum possible value in above focusing current condition. The minimum value of response is observed at the inverse condition, wherein for the same voltage, the focus current is at a minimum possible value in below focus condition. This lower value of responses is usually a condition of undercut for bead height and a condition involving cavity for bead width. Hence, an optimum combination of focusing current and voltage is necessary to be found, for which SS304 is observed to be at surface focus condition for a particular voltage.

   Figure 9 shows the surface and contour plots depicting the interaction between focusing current and accelerating voltage with respect to response BP. Similar effects are seen in case of BBW. The plots again clearly indicate a linear relation between the two predictors with focusing current increasing as accelerating voltage increases, but their effect on the response variable BP and BBW is inverse to the one observed for BH and BW. The behavior of these input parameters was expected as it was indicated by the correlation analysis in the initial stages

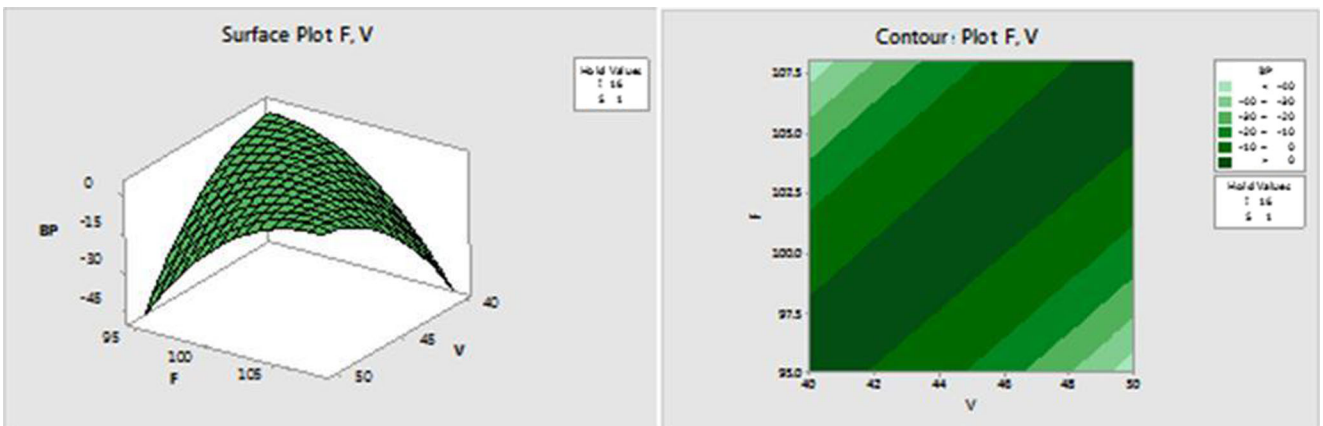

Fig. 9 Surface and contour plots of *F*-*V* interaction for BP

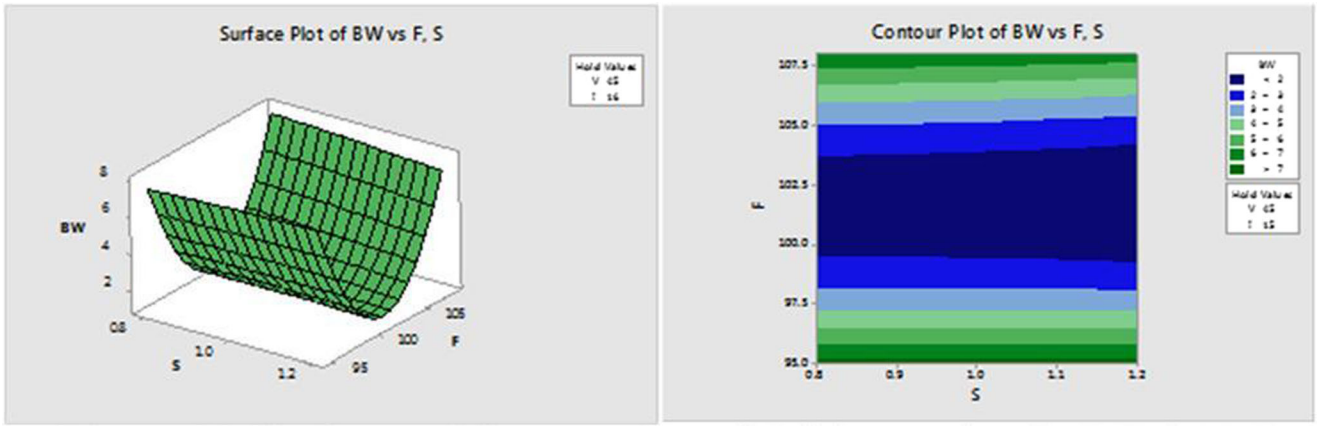

Fig. 10 Surface and contour plots of *F*-*S* interaction for BH

of model development. The responses BP and BBW are seen to be least when for a particular voltage, the focusing current is at a maximum possible value in above focusing current condition. The maximum value of response is observed at the inverse condition, wherein for the same voltage, the focus current is at a minimum possible value in below focus condition. This lower value of responses is usually a condition of partial penetration for response BP with no visible BBW. Hence, an optimum combination of focusing current and voltage was necessary to be found, for which SS304 was observed to be at surface focus condition for a particular voltage.

2. Focusing current (*F*) and welding speed (*S*)

Figure 10 shows the surface and contour plots depicting the interaction of focusing current and welding speed with respect to response BH. Similar effects are seen in case of BW. Similarly, Fig. 11 shows the surface and contour plots depicting the interaction between focusing current and accelerating voltage with respect to response BP with similar effects seen in case of BBW. The most important observation made in these interaction plots is that any change in welding speed for a particular focusing current at a certain voltage has a very marginal effect on the response variables. Whereas for a particular welding speed, any change in the focusing current brings about a linear change in the response variables.

Another deduction from these plots is that for above focusing current values, increasing the welding speed tends to decrease the responses BH and BW, whereas BP and BBW tends to increase and vice versa. In a below focus condition, the responses show very minimal variation for any change in welding speed. The minimum values of BH and BW and maximum values for BP and BBW are obtained around a surface focusing condition. This behavior of welding speed makes it one of the best parameters for making minor adjustments in the response values.

3. Focusing current (*F*) and beam current (*I*)

Figure 12 shows the surface and contour plots depicting the interaction of focusing current and beam current with respect to response BH. Similar effects are seen in case of BW. Similarly, Fig. 13 shows the surface and contour plots depicting the interaction between

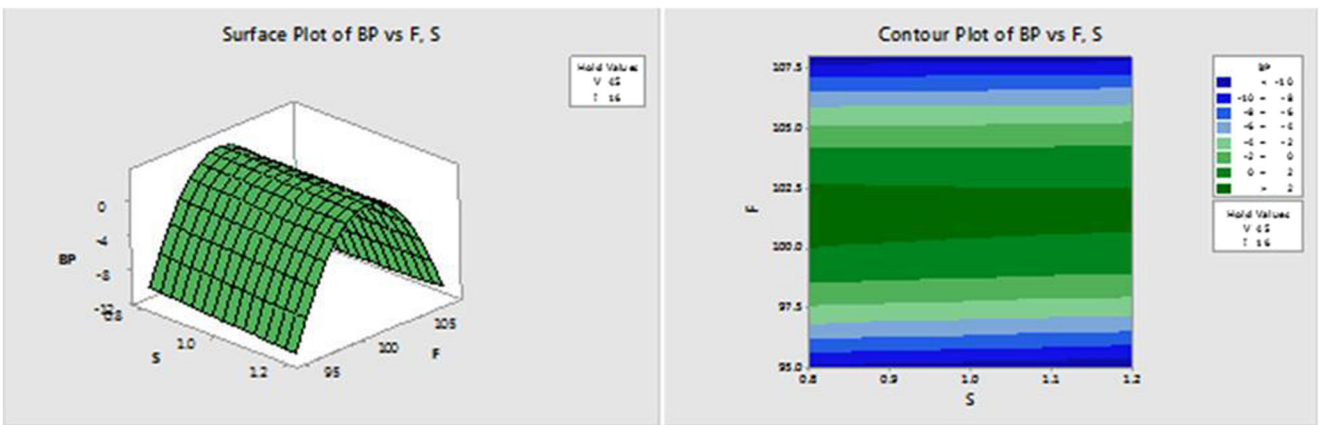

Fig. 11 Surface and contour plots of *F*-*S* interaction for BP

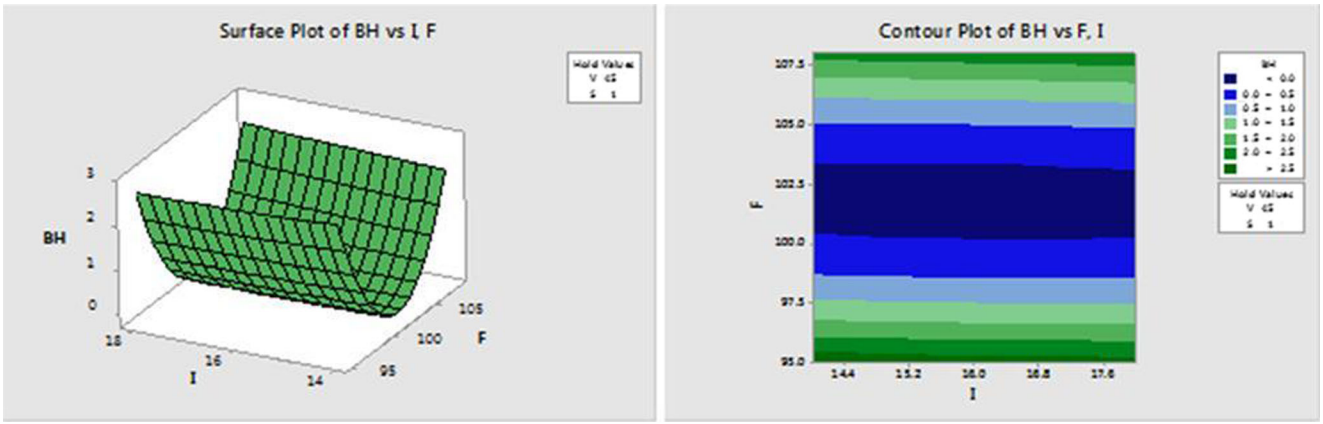

Fig. 12 Surface and contour plots of *F-I* interaction for BH

focusing current and beam current with respect to response BP with similar effects seen in case of BBW. It is obvious from the plots that the interaction effects of these two input parameters are very similar to focusing current and welding speed. The most important observation made in this interaction is that any change in beam current for a particular focusing current at a certain voltage has a marginal effect on the response values. This is significantly more than the changes brought about by welding speed in the response variables. For a particular beam current, any change in the focusing current brings about a very significant linear change in the response values.

Another deduction from these plots is that for above focusing current values, increasing the beam current tends to decrease the responses BH and BW, whereas BP and BBW tends to increase and vice versa. In a below focus condition, the responses show minimal variation for any change in beam current. The minimum values of BH-BW and maximum values for BP-BBW are obtained around a surface focusing condition. This behavior of beam current makes it also one of the best parameters for making minor adjustments in the response values.

5.5 Optimization using genetic algorithm

The estimated global minima for BH, BW, and BBW responses along with maxima of BP are reported in Table 8.

Figure 14 shows the four major output plots for optimization of responses, which indicate the fitness values (optimum) for each computed generation and the global extrema (indicated as "best") of BH, BW, BP, and BBW.

Further, the minimization of SS304 weld bead cross-sectional area resulted in a minima of bead area as 1.447 mm^2 with a response parameter combination of [BH, BW, BP, BBW] as [0.151, 1.053, 2.143, 0.158]. When this value was compared to the cross-sectional area measured of a specimen from the full factorial DOE data with a just penetrated condition of the bead, the weld bead was seen to have an area of 1.47 mm^2. This optimized overall best fit value is undoubtedly the minimized weld bead area.

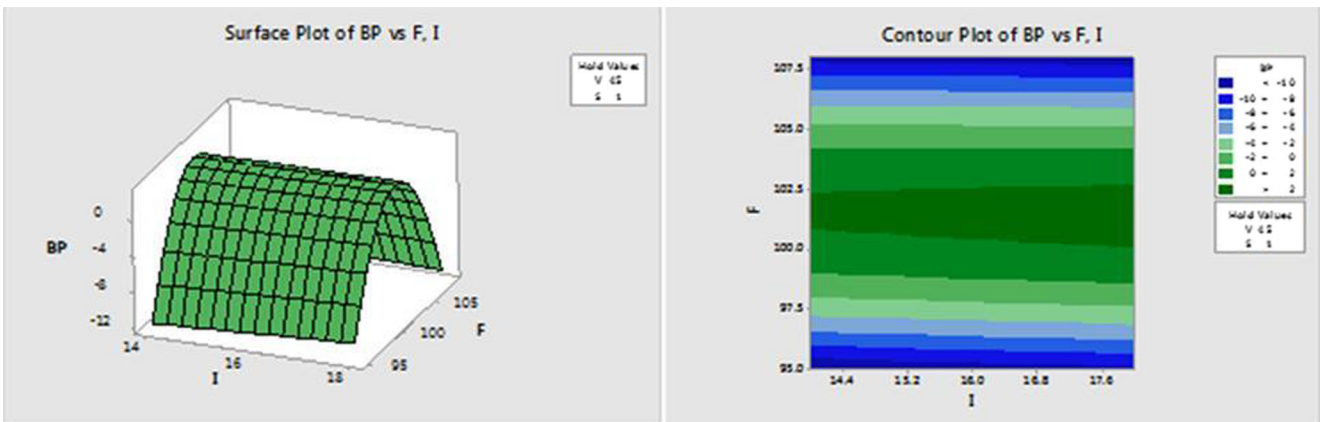

Fig. 13 Surface and contour plots of *F-I* interaction for BP

Table 8 Optimized data report of each bead response variable

SS304 bead optimization		*V* (kV)	*I* (mA)	*S* (m/min)	*F* (A)	Extremum response (mm)	Number of iterations to achieve extremum
Minimization of SS304 bead height (BH)	GA minima	50	16	0.88	106.8	−0.04	51
	Experimental minima	50	16	1	106	−0.04	–
Minimization of SS304 bead width (BW)	GA minima	40	14.5	1.2	96	1.05	51
	Experimental minima	40	18	1.2	96	1.1	–
Maximization of SS304 bead penetration (BP)	GA maxima	40	18	0.83	95.8	2.77	60
	Experimental maxima	40	18	0.8	95	2.77	–
Minimization of SS304 back bead width (BBW)	GA minima	40	18	0.9	97	0.16	57
	Experimental minima	40	16	1	96	0.18	–

Figure 15 shows the GA output for the minimization of EB weld bead cross-sectional area as computed on MATLAB 7.0 210a; it shows

- The fitness plot with an overall best fit value of 1.447.
- Plot indicating the average distance between individuals, where the uniform pattern in the plot indicates the fact that the model is not getting trapped in any of the local minima before it has reached the global minima. It also indicates that each generation is better than the previous generation, hence getting closer to the desired optimal value.
- The best individual plot, where as expected the bead penetration response (3) is the best individual, as it has a fractionally a bigger contribution in the bead area, followed by the bead width (2), then by the bead height (1), and finally, the back bead width (4).
- Best, worst, and maximum score plots, where the plot shows that the difference between the results from one

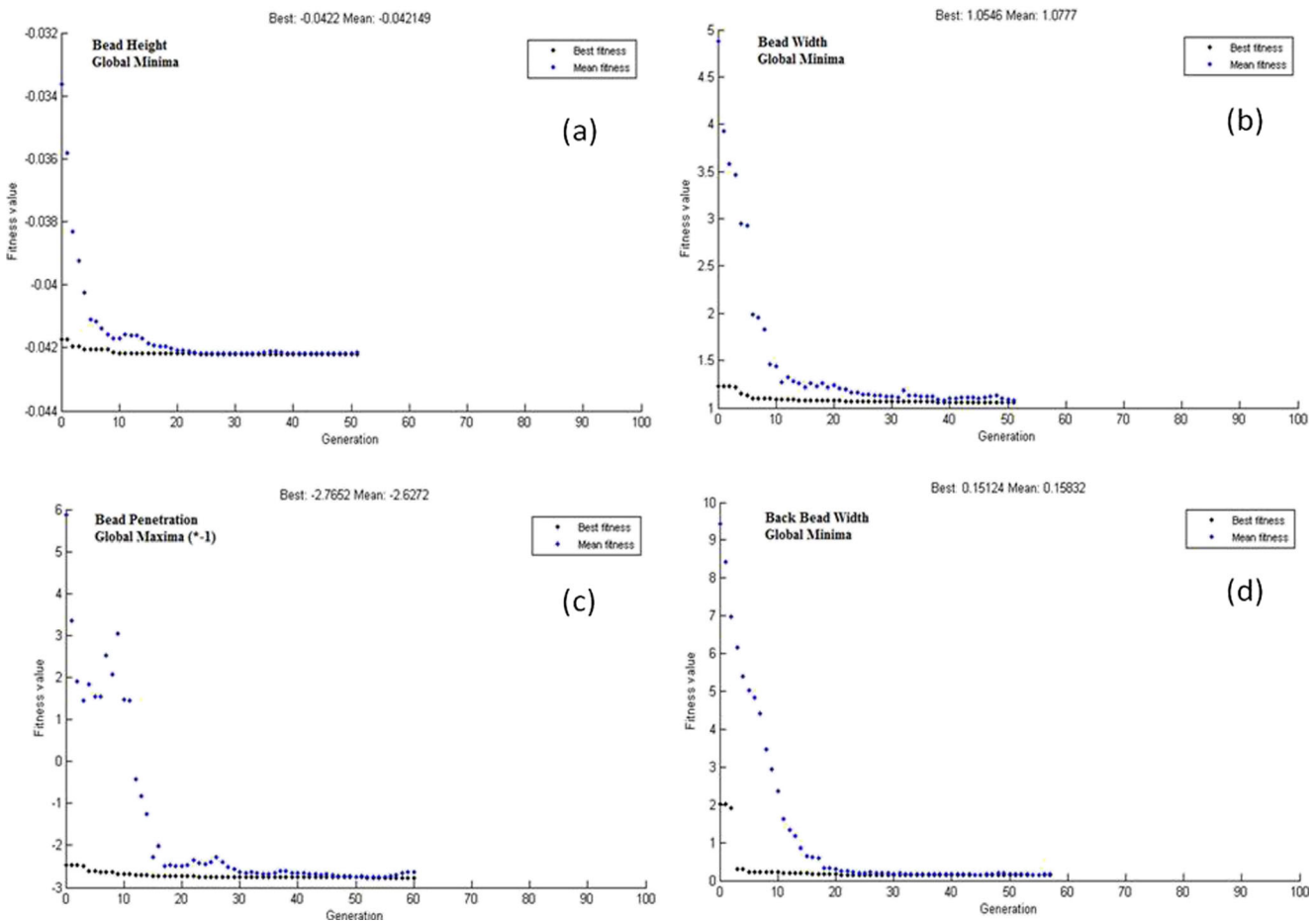

Fig. 14 GA analysis, fitness values vs generation plots of each response variable with indication of respective best value and extremum

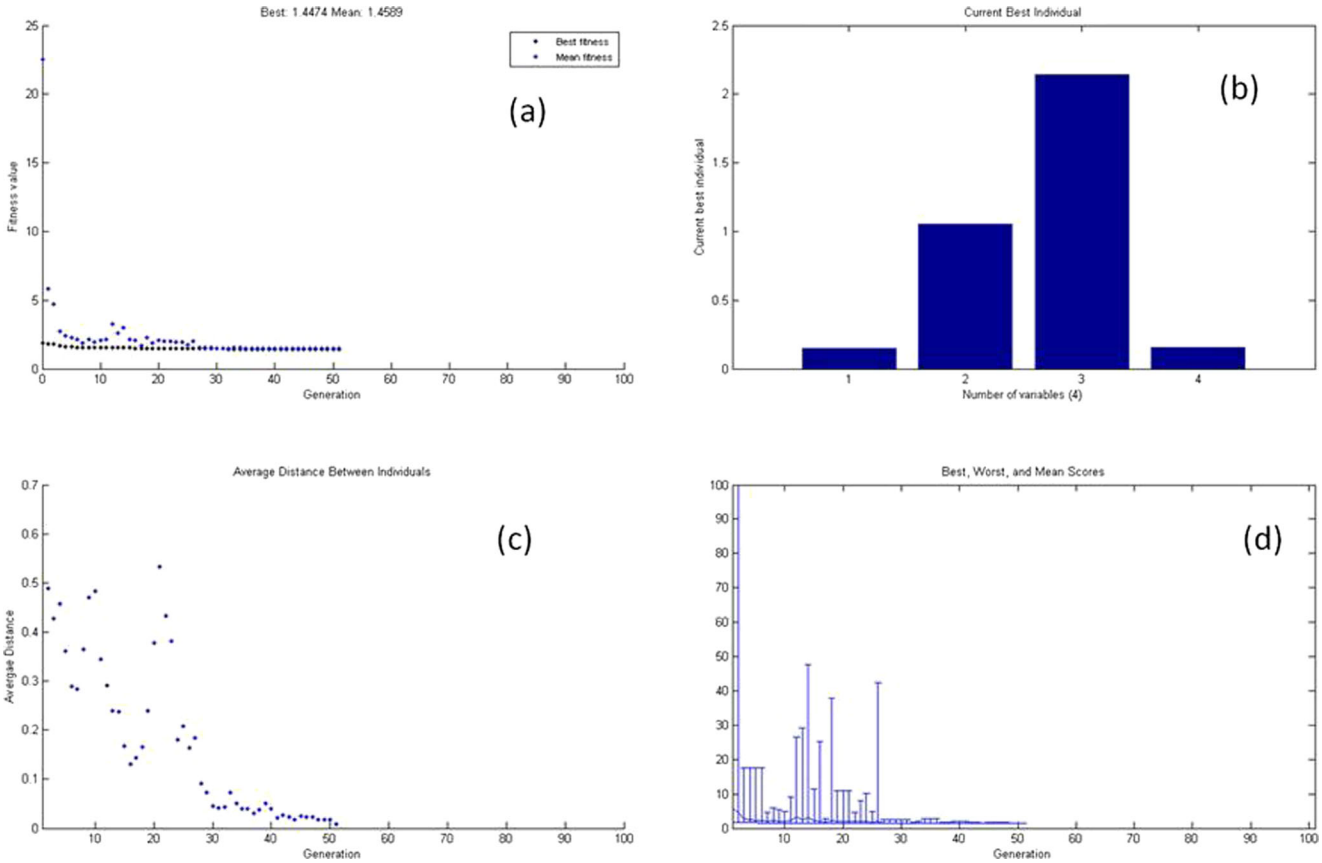

Fig. 15 GA minimization output for weld bead cross-sectional area

generation to the next is not fluctuation uncontrollably. It also indicated that this difference is progressively becoming negligible, reaching the required optimum value at 51st iteration.

6 Conclusion

The present study was able to automate and standardize the weld initialization process for the electron beam welding of 304 stainless steel. This in turn has resulted in increased productive man hours on the shop floor, reduced manufacturing lead time, and eliminated unnecessary reworks and quality control cycles.

This has been achieved by eliminating the time-consuming trail error-based method of estimating EB weld parameters, which was purely based on the expertise of the EB weld machine operator. The success and quality of this were not assured unless extensive weld quality checks were carried out. The model presented has successfully replaced this trial error method with a meticulously built mathematical model that is able to relate the bead geometry with the EB weld input parameters. This way, actual welds need not be carried out to find the best welding parameters for the given specifications. Through extensive weld quality checks, the study also proves the adequacy of the model optimized through genetic algorithm, which provides a weld bead with minimum cross-sectional area achievable and hence a minimal HAZ without compromising on the quality of weld.

The developed mathematical model can predict the weld bead geometry for electron beam butt welding of 2-mm-thick SS304 plates with high repeatability at an accuracy of 91.7 %. This model has been able to incorporate the effect of focusing current in developing a relation between the welding parameters and the bead geometry. The study brings out the significance of interactions within the input parameters and the effect they have on the bead geometry.

This study also eliminates the cumbersome manual usage of resultant equations for predicting the response variables of EB welding whenever required. This was done by developing a graphical user interface (GUI) on MATLAB 7.0 using the GUDE toolbox. With this interface, predicting the bead geometry is as simple as addition operation on a calculator. The user only needs to enter the EB weld input variables, and the interface does the rest of the substitution and computational work, providing the bead dimensions as output with necessary plots to analyze the results.

Acknowledgments The authors would like to express their sincere gratitude to Shri. Sibnath Som, Director, DRDL, Hyderabad, and Department of Production Engineering, Birla Institute of Technology, Mesra, Ranchi, for their constant support to carry out this experiment. The authors also thank the Head Material Development Division (MDD) at DRDL for his constant support to carry out the material characterization part and mechanical testing. The authors would like to extend a special thanks to Mrs. Meenakshi Patil, Mr. Naveen Kumar, and all technicians at Special Fabrication Division workshop.

References

1. Benyounis K, Olabi A (2008) Optimization of different welding processes using statistical and numerical approaches—a reference guide. Adv Eng Softw 39(6):483–496
2. Dashatan SH, Azdast T, Ahmadi SR, Bagheri A (2013) Friction stir spot welding of dissimilar polymethyl methacrylate and acrylonitrile butadiene styrene sheets. Mater Des 45:135–141
3. David SA, Vitek JM, Rappaz M, Boatner LA (1990) Microstructure of stainless steel single-crystal electron beam welds. Metall Trans A 21(6):1753–1766. doi:10.1007/BF02672592
4. Dey V, Pratihar D, Datta G, Jha MN, Saha TK, Bapat AV (2010) Optimization and prediction of weldment profile in bead-on-plate welding of Al-1100 plates using electron beam. Int J Adv Manuf Technol 48(5–8):513–528
5. Dey V, Pratihar DK, Datta GL, Jha MN, Saha TK, Bapat AV (2009) Optimization of bead geometry in electron beam welding using a genetic algorithm. J Mater Process Technol 209(3):1151–1157
6. Henderson MB, Arrell D, Larsson R, Heobel M, Marchant G (2004) Nickel based superalloy welding practices for industrial gas turbine applications. Sci Technol Weld Join 9(1):13–21. doi:10.1179/136217104225017099
7. Holland JH (1992) Adaptation in natural and artificial systems: an introductory analysis with applications to biology, control, and artificial intelligence. A Bradford book. MIT Press, Cambridge
8. Jean MD, Wang JT (2006) Using a principal components analysis for developing a robust design of electron beam welding. Int J Adv Manuf Technol 28(9–10):882–889. doi:10.1007/s00170-004-2219-z
9. Jha MN, Pratihar DK, Dey V, Saha TK, Bapat AV (2011) Study on electron beam butt welding of austenitic stainless steel 304 plates and its input–output modelling using neural networks. Proc Inst Mech Eng B J Eng Manuf 225(11):2051–2070
10. Rawlings JO, Pantula SG, Dickey DA (2001) Applied regression analysis: a research tool. Springer, New York
11. Kelly Ferjutz JRD (1993) ASM handbook: volume 6: welding, brazing, and soldering. ASM International, Materials Park
12. Khan Z, Prasad B, Singh T (1997) Machining condition optimization by genetic algorithms and simulated annealing. Comput Oper Res 24(7):647–657
13. Klykov NA, Dammer AA, Druzhinin AV, Malysh MM (1987) Calculations of the form of the penetration zone in laser welding using a model of two heat sources. Weld Int 1(10):914–916
14. Koleva E, Vuchkov I (2005) Model-based approach for quality improvement of electron beam welding applications in mass production. Vacuum 77(4):423–428
15. Li Z, Gobbi SL, Bonollo F, Tiziani A, Fontana G (1998) Metallurgical investigation of laser welds in wrought Waspaloy. Sci Technol Weld Join 3(1):1–7
16. Li Z, Gobbi SL, Loreau JH (1997) Laser welding of Waspaloy® sheets for aero-engines. J Mater Process Technol 65(1–3):183–190
17. Madhusudan RG, Rao KS (2009) Microstructure and mechanical properties of similar and dissimilar stainless steel electron beam and friction welds. Int J Adv Manuf Technol 45(9–10):875–888. doi:10.1007/s00170-009-2019-6
18. Sanderson A (2007) Four decades of electron beam development at TWI. Weld World 51(1–2):37–49. doi:10.1007/BF03266547
19. Bauer B, Busic M (2015) High energy density welding process. In: Kralj S (ed) Welding engineering and technology. EOLSS Publishers Co Ltd., Ramsey, Isle of Man, Chapter 6, p 2–3
20. Schultz H (2003) Electron beam welding. Woodhead Publishing, Cambridge
21. Wang S, Wu X (2012) Investigation on the microstructure and mechanical properties of Ti–6Al–4V alloy joints with electron beam welding. Sustain Mater Des App 36:663–670. doi:10.1016/j.matdes.2011.11.068